Article

The Role of Lead (Pb) in the High Temperature Formation of MoS$_2$ Nanotubes

Olga Brontvein [1], Reshef Tenne [1] and Andrey Enyashin [2],*

[1] Department of Materials and Interfaces, Weizmann Institute of Science, Rehovot 7610001, Israel;
E-Mails: olga.brontvein@weizmann.ac.il (O.B.); reshef.tenne@weizmann.ac.il (R.T.)

[2] Institute of Solid State Chemistry RAS Pervomayskaya Str., 91, 620990 Ekaterinburg, Russia

* Author to whom correspondence should be addressed; E-Mail: enyashin@ihim.uran.ru;
Tel.: +7-343-362-3115; Fax: +7-343-374-4495.

Abstract: Recent studies have clearly indicated the favorable effect of lead as a growth promoter for MX_2 (M = Mo, W; X = S, Se) nanotubes using MX_2 powder as a precursor material. The experimental work indicated that the lead atoms are not stable in the molybdenum oxide lattice ion high concentration. The initial lead concentration in the oxide nanowhiskers (Pb:Mo ratio = 0.28) is reduced by one order of magnitude after one year in the drawer. The initial Pb concentration in the MoS$_2$ nanotubes lattice (produced by solar ablation) is appreciably smaller (Pb:Mo ratio for the primary samples is 0.12) and is further reduced with time and annealing at 810 °C, without consuming the nanotubes. In order to elucidate the composition of these nanotubes in greater detail; the Pb-"modified" MX_2 compounds were studied by means of DFT calculations and additional experimental work. The calculations indicate that Pb doping as well as Pb intercalation of MoS$_2$ lead to the destabilization of the system; and therefore a high Pb content within the MoS$_2$ lattice cannot be expected in the final products. Furthermore; substitutional doping (Pb$_{Mo}$) leads to p-type semiconducting character; while intercalation of MoS$_2$ by Pb atoms (Pb$_y$/MoS$_2$) should cause n-type semiconducting behavior. This study not only sheds light on the role of added lead to the growth of the nanotubes and their role as electron donors; but furthermore could pave the way to a large scale synthesis of the MoS$_2$ nanotubes.

**Keywords:** inorganic nanotubes; high temperature synthesis; DFT calculations

1. Introduction

Inorganic nanotubes (INT) have become a prominent research subject in recent years. Their unique mechanical, optical and electrical properties [1–8] prompted extensive investigation. A number of synthetic routes have been developed, for example, chemical vapor transport using bromine for INT-MoS$_2$ [9,10], bismuth catalyzed vapor-liquid-solid method for SnS$_2$ nanotubes [11], misfit compounds superstructures of SnS-SnS$_2$ and NbS-PbS$_2$ nanotubes [12,13] and sulfidization of tungsten suboxide nanowhiskers leading to the formation of INT-WS$_2$ [14].

Recent studies have shown a new strategy for successful synthesis of *MX*$_2$ (*M* = Mo, W; *X* = S, Se) nanotubes using Pb as a growth promoter [15,16]. Figure 1 presents a SEM image of MoS$_2$ nanotubes (Figure 1a) and high resolution TEM image of single MoS$_2$ nanotube (Figure 1b) formed by irradiating MoS$_2$ powder by a focused (×15,000) sunlight for 10 min [15]. The inset in Figure 1b shows the distance profile of nanotube layers. The interlayer spacing of 0.634 nm is somewhat larger than that of bulk 2H-MoS$_2$ (0.62 nm). This 2% expansion of the lattice spacing in the nanotubes is well documented [17] and is attributed to strain relaxation. Figure 1c shows the EDS spectrum of single MoS$_2$ nanotube after the irradiation, the table in the inset in Figure 1c shows the atomic % of the elements. In both cases the formation mechanism can be described as a Pb-promoted *MX*$_2$ conversion into Mo(Pb)O$_{3-x}$ nanowhiskers at high temperature (>2500 °C). Once formed, the nanowhiskers react back with the X-vapor which leads to the formation of *MX*$_2$ nanotubes. Numerous attempts to synthesize MoS$_2$ nanotubes in a conventional oven (up to 1000 °C) or induction furnace (up to 1600 °C), with the same precursor materials, or generation of Mo(Pb)O$_{3-x}$ nanowhiskers and their subsequent sulfidization did not succeed. It appears, therefore, that the high temperatures (>2500 °C) and the presence of lead are critical for the conversion of MoS$_2$ powder into Mo(Pb)O$_{3-x}$ nanowhiskers which serve as template for the synthesis of *MX*$_2$ nanotubes according to this process. In addition, the use of Pb as a growth promoter is environmentally unfavorable. Therefore, stabilization of molybdenum suboxide phases could be done using different metals, for example V, Ta or W [18–20].

The main goal of the current work is to understand the role of lead (Pb) as a growth promoter of INT-MoS$_2$; evaluate its solubility limits in the two lattices (oxide and sulfide) and their electronic state in the INT-MoS$_2$ lattice. In particular, the stability of this heavy metal in the oxide precursor and the formed MoS$_2$ nanotubes was investigated through both theory and experiment. Due to the fast kinetics of the process, the samples (oxide nanowhiskers and nanotubes) formed in such extreme conditions contain a certain amount of Pb. However, the content of Pb is found to be time-dependent and can considerably decrease upon thermal annealing. DFT calculations give preliminary information about the coordination and the electronic state of Pb atoms within the MoS$_2$ lattice. They verify a low affinity of the Pb atoms as dopants or intercalants in the sulfide matrices and indicate that the experimentally observed high amount of lead (Pb) is too far from the thermodynamic equilibrium conditions.

Figure 1. MoS$_2$ nanotubes formed using solar ablation system (**a**) SEM image of MoS$_2$ nanotubes; (**b**) high resolution TEM image of a single MoS$_2$ nanotube (adapted after [15]). The inset shows the profile of the interlayer distances of the nanotube wall. The interlayer spacing is somewhat larger than that of bulk 2H-MoS$_2$ (0.62 nm); (**c**) EDS spectrum of a single MoS$_2$ nanotube; the inset table shows atomic % of the nanotube's elements.

| Element	Atomic %
O	17.2
S	50.5
Pb	1
Mo	31.3
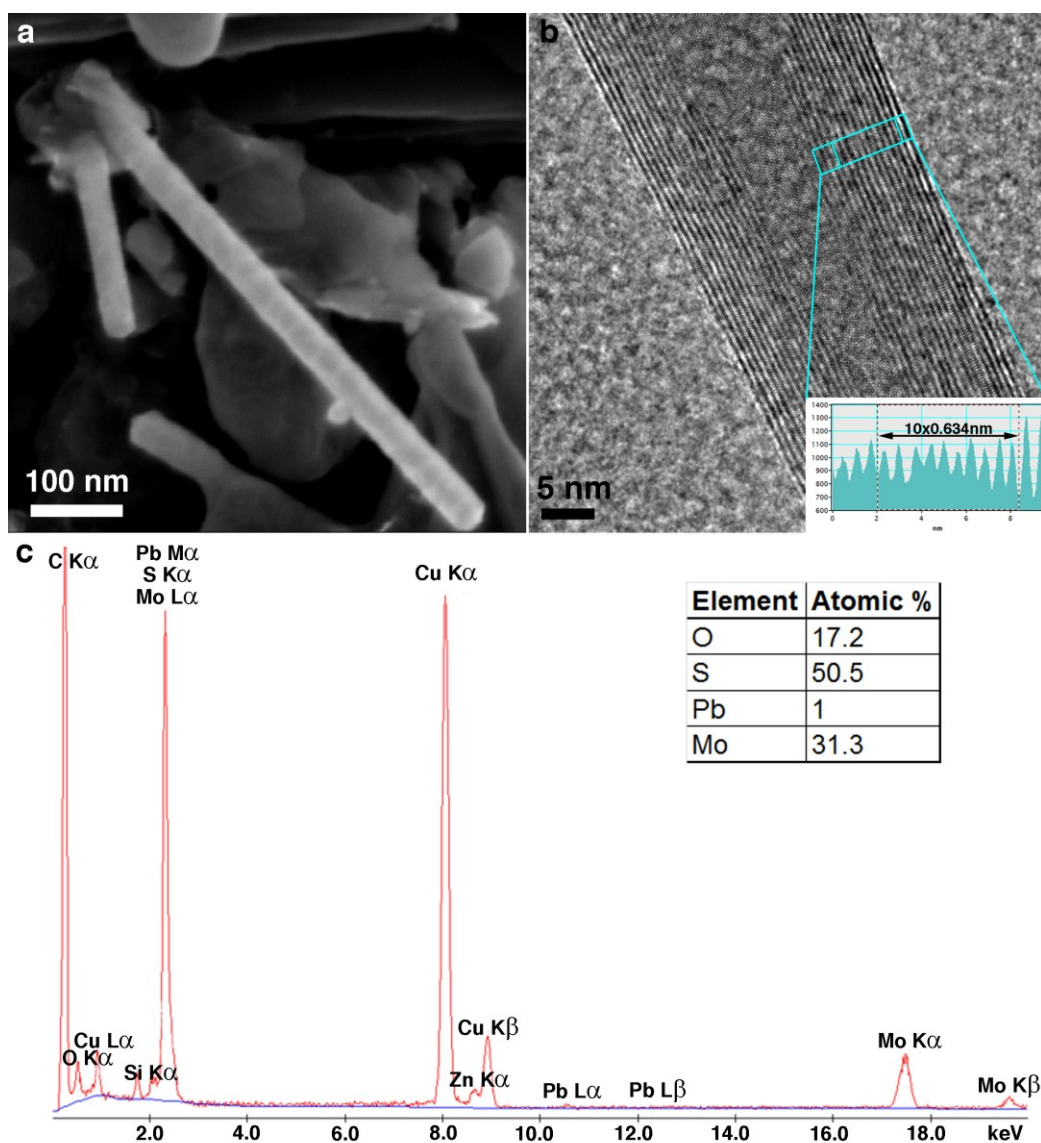
2. Results and Discussion

2.1. Annealing

To distinguish between the different samples of oxide nanowhiskers and the molybdenum disulfide nanotubes studied in this work a labeling system was used (see Table 1). For this work, two different precursors were investigated: MoO$_{3-x}$ (2) nanowhiskers and MoS$_2$ (2) nanotubes, which were left one year in the drawer after solar ablation synthesis. The detailed description of their synthesis can be seen in the experimental part. Due to the small quantities of the MoS$_2$ nanotubes and MoO$_{3-x}$ nanowhiskers that are obtained in the synthesis (~1%–2% yield) only single particle EDS measurement can be suitable for their chemical analysis.

Table 1. The samples labeling that were used during the experimental work.

Precursor	After the Solar Ablation Synthesis	After a Year in Ambient Conditions	30 min Annealing in H_2S	1 h Annealing in H_2S	2 h Annealing in H_2S
MoO_{3-x}	MoO_{3-x} (1)	MoO_{3-x} (2)	MoS_2 (3a)	MoS_2 (3b)	MoS_2 (3c)
MoS_2	MoS_2 (1)	MoS_2 (2)	MoS_2 (4a)	MoS_2 (4b)	MoS_2 (4c)

The experimental work which has recently been carried-out indicated that the Pb atoms are not stable in high concentrations in the MoO_{3-x} or MoS_2 lattice. According to the EDS measurements the initial lead concentration in the molybdenum suboxide nanowhiskers MoO_{3-x} (1) was reduced by one order of magnitude after one year in the drawer (Pb:Mo ratio reduced from ~0.28 to 0.03 in MoO_{3-x}(2)) (Figure 2). The same analysis showed that in the case of MoS_2 (1) nanotubes the Pb concentration decreased from ~0.12 to 0.03 in MoS_2; (2). Subsequent annealing of both types of nanostructures, *i.e.*, MoO_{3-x} (2) nanowhiskers and MoS_2 (2) nanotubes, leads to additional reduction of the Pb concentration. The Pb:Mo ratio before and after annealing calculated from EDS measurements can be seen in Figure 2. It should be emphasized that the accuracy of the EDS is greatly compromised at the lower concentration limit of Pb.

Figure 2. Pb:Mo ratio of the precursors and products according to the EDS measurements, (**a**) MoO_{3-x} (2) nanowhiskers as a precursor material; (**b**) MoS_2 (2) nanotubes as a precursor material.
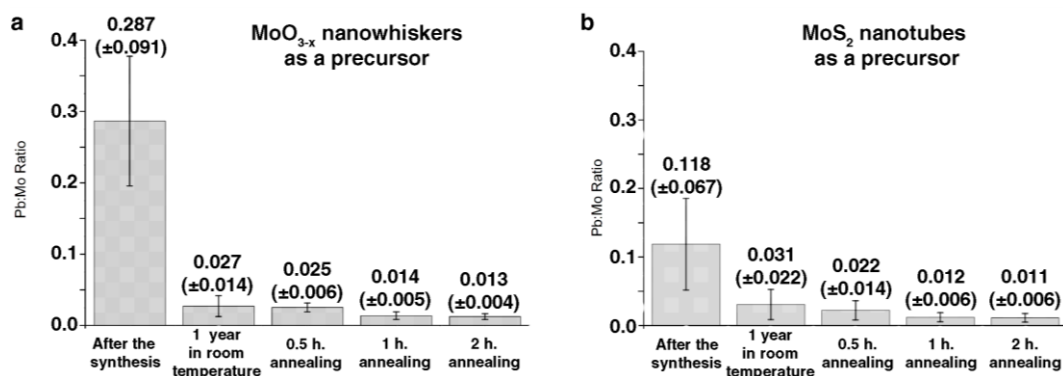
The outdiffusion of the lead from the molybdenum oxide nanowhiskers MoO_{3-x} (2) did influence their high-temperature stability and their conversion into MoS_2 (3) nanotubes upon annealing in H_2S atmosphere at 810 °C. In all cases, MoS_2 (3,4) nanotubes were observed after the sulfidization and annealing of the lead-depleted MoO_{3-x} (2) nanowhiskers and MoS_2 (2) nanotubes. TEM images of the precursors and products can be seen in Figure 3. Detailed description of the annealing conditions can be seen in the experimental section.

Due to the overlap between the Mo(L) and Pb(M) peaks (2.3 KeV) in the EDS spectra, the calculated atomic concentration of Pb is based on the Pb(L) (10.5 KeV) and Mo(K) (17.4 KeV) peaks, which provide lower accuracy. Therefore, the detection of Pb atoms after a year in the drawer is limited to the detected range (>0.2 at%). On the other hand, it can be seen from the EDS spectra of the samples before and after annealing that in the case of molybdenum suboxide nanowhiskers MoO_{3-x} (2) as a precursor material, the Pb peak disappears after two hours annealing in H_2S atmosphere, while the same peak disappears after 30 min annealing at 810 °C in the case of MoS_2 (2) nanotubes (Figure 4).

Figure 3. TEM images, (**a**) MoO_{3-x} (1) nanowhisker obtained after the synthesis (solar ablation for 30 s); (**b**) MoO_{3-x} (2) nanowhisker a year after the synthesis; (**c–e**) MoS_2 (3) nanotubes after 30 min, 1 and 2 h of H_2S annealing, respectively, with MoO_{3-x} nanowhiskers as a precursor; (**f**) MoS_2 (1) nanotubes after the synthesis (solar ablation for 10 min); (**g**) MoS_2 (2) nanotube a year after the synthesis, (**h–j**) MoS_2 (4) nanotubes after 30 min, 1 and 2 h (H_2S) annealing, respectively, with MoS_2 (2) nanotubes as a precursor.
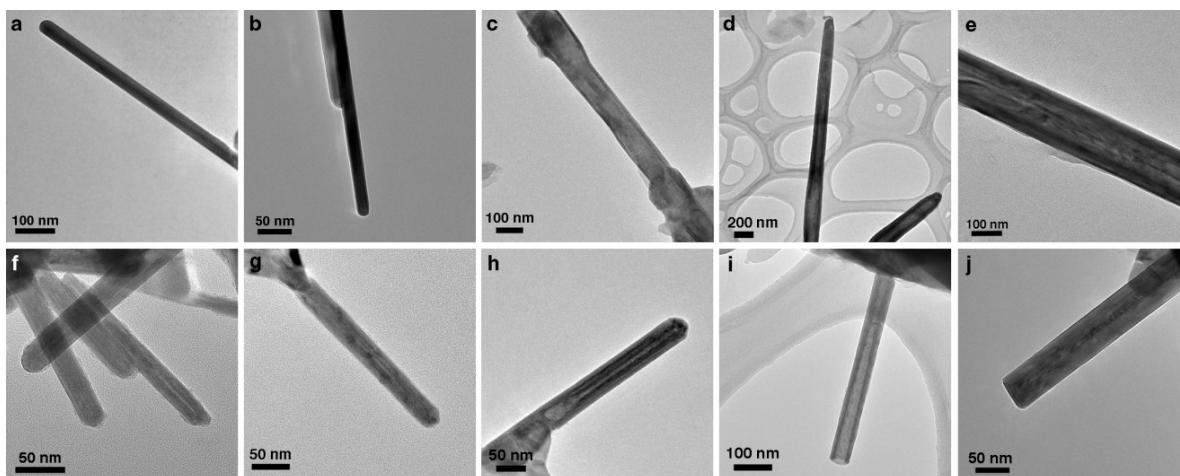

Figure 4. EDS spectra of the samples before and after annealing at 810 °C, (**a**) MoO_{3-x} (2) nanowhiskers as a precursor; (**b**) MoS_2 (2) nanotubes as a precursor.
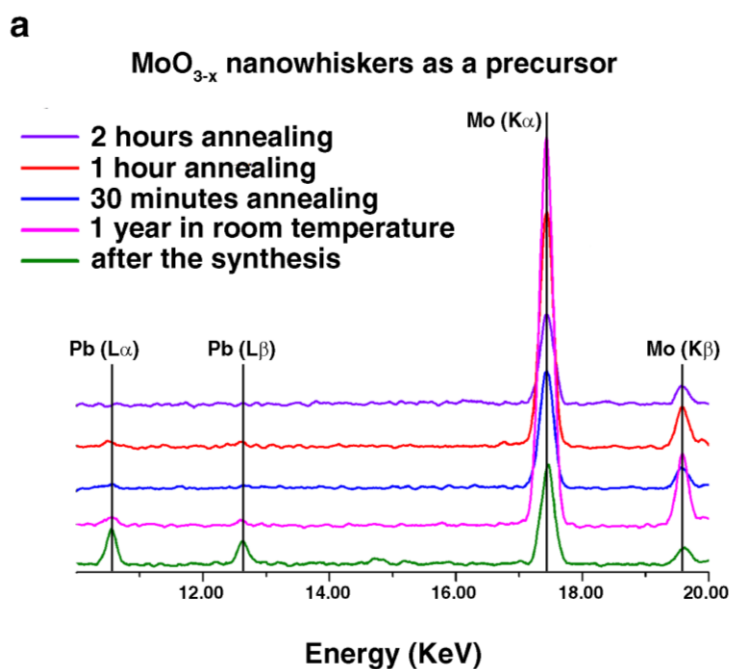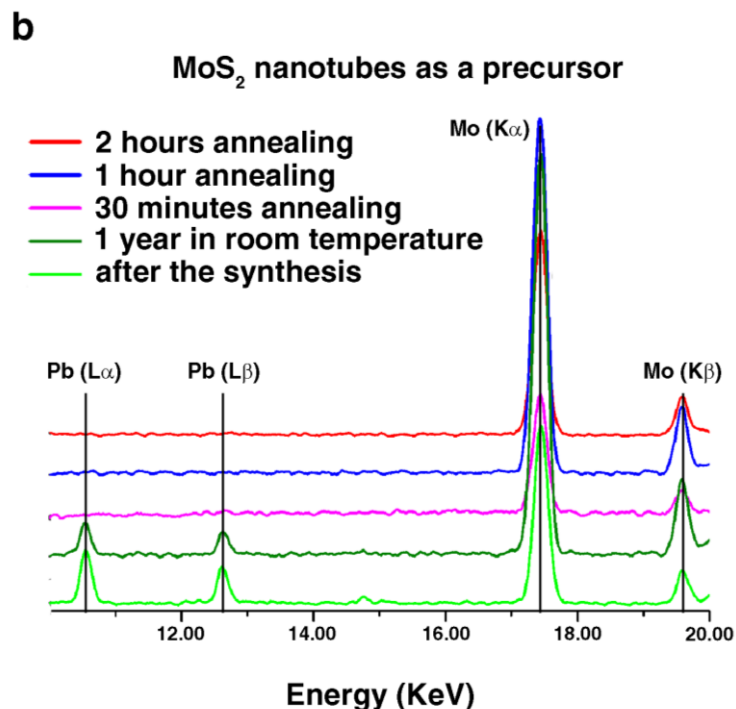
Figure 4. *Cont.*

b

MoS₂ nanotubes as a precursor

*2.2. DFT Calculations of Mo₁₋ₓPbₓS₂ Solid Solutions and Pbᵧ/MoS₂ Intercalates*

The experimental work has indicated a time-dependent content of Pb in the samples of MoS₂ nanotubes after Pb-promoted synthesis, which suggests that the MoS₂ lattice forms an unfavorable environment for the Pb atoms in these nanostructures. In order to elucidate preliminary the accommodation type, chemical bonding and the highest possible (at equilibrium) concentration of Pb atoms in the samples of MoS₂ nanotubes a set of DFT calculations were performed. Two cases were considered: (1) the lead atoms substitute the Mo in the lattice and serve as dopants ($Mo_{1-x}Pb_xS_2$ solid solutions); (2) the Pb atoms intercalate into the interlayer space of the MoS₂ host lattice (Pb_y/MoS_2 intercalates).

2.2.1. Electronic Structure

Test DFT calculations at LDA level were performed on example of the bulk 2H-MoS₂ and fcc-PbS crystals (see Section 3). 2H-MoS₂ was found to be a semiconductor with direct band gap 2.18 eV and indirect $\Gamma \rightarrow \frac{1}{2}K\Gamma$ gap of 0.59 eV. The valence band is composed mainly of S3p-states, about ~3.5–6.0 eV below the Fermi level. The top of the valence band and the bottom of the conduction band are dominated by Mo4d-states. In the electronic structure of fcc-PbS the occupied Pb6s band is present between 6.5 and 9.5 eV below the Fermi level. The three predominately S3p bands are located between −6 and 0 eV. The fundamental band gap of 0.11 eV is direct at the L point with the conduction band composed predominately of Pb6p states. While the values of the band gaps are also typically underestimated in LDA approach, the band structures are in full accordance with other theoretical and experimental results [21,22].

In general, the band structure of MoS_2 and the corresponding picture of the densities of states (DOS) are essentially not perturbed by substitutional doping of the Mo sublattice by a single Pb atom (Figure 5a). A single level separates from the bottom of the conduction band into the band gap of pristine MoS_2, while the Fermi energy shifts downwards the top of valence band. In addition, a new level emerges at 1 eV below the bottom of the valence band of doped MoS_2. It is composed mainly of Pb6*s* states, which do not overlap with the S3*p* band and do not contribute to the chemical bonding of the system. Thus, like in the case of PbS compound, the chemical bonding of Pb atom with S atoms is released due to the depopulation of only Pb6*p* states, which can be found at 5–6 eV above the Fermi energy. All these features are evidence for a p-type semiconducting character of the Pb-doped MoS_2 and nominal 2+ oxidation state of Pb. Such oxidation state and the arising electron deficiency of MoS_2 electronic structure should lead to destabilization of the chemical environment of the Pb-doped MoS_2 lattice. The map of the differential electron densities for this system supports this deduction and demonstrates a vanishing electron density and weakening of the bonds near the Pb atom compared to the electron density nearby the Mo atoms (Figure 5a).

Figure 5. (**a**) Band structure; electronic partial densities of states (DOS) for Pb and differential electron density map for 2H-MoS_2 crystal doped by single Pb atom; (**b**) Band structure, DOS for Pb and differential electron density map for 2H-MoS_2 crystal intercalated by single Pb atom. LDA DFT calculations.
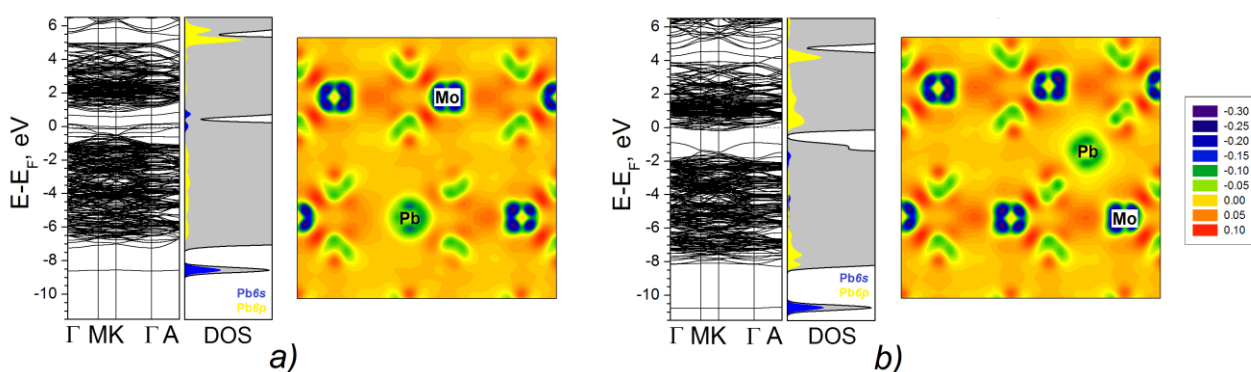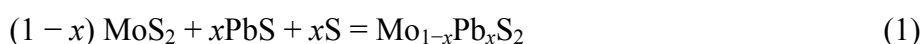

Another possible process, which could occur during the Pb-promoted growth of MoS_2 nanotubes, is an intercalation of MoS_2 lattice by Pb atoms. The intercalation by a single Pb atom also does not affect the band structure essentially (Figure 5b). Yet, in this case the Fermi level shifts upwards into the conduction band. The localized Pb6*s* states occur deeper at 2 eV below the bottom of valence band. Pb6*p* states of the intercalating Pb atom are more delocalized within the conduction band, than in the aforementioned case of Pb doping. Thus, a Pb_y/MoS_2 intercalate should behave as an n-type semiconductor. The map of differential electron density for this system does not reveal any essential covalent bond formation with S atoms and serves as an evidence for the non-amicable environment of the intercalating Pb atoms.

2.2.2. Estimation of the Stability Limit for Lead Atoms in the MoS$_2$ Lattices

Both doping and intercalation by single Pb atoms lead to a destabilization of the MoS$_2$ electronic system. A weakening of the chemical bonding within the MoS$_2$ lattice due to electron deficiency of the valence band or occupation of anti-bonding Mo4d-states, are observed, respectively. A stabilization of the lattice is not favored also by the sterical strain induced after the difference in the radii between Mo and Pb atoms. e.g., optimized lattice parameters for substitutionally Pb-doped MoS$_2$ lattice reveal a slight increase of the lattice parameter a from 3.12 Å to 3.15 Å due to the single Pb impurity atom and up to 3.19 Å due to the "cluster" of four Pb atoms. The interlayer distance is not considerably affected in both cases and is ~0.05 Å smaller, than in the pure 2H-MoS$_2$. The intercalation of MoS$_2$ lattice by individual Pb atoms has opposite effect: the a lattice parameter is increased by ~0.01 Å, while the interlayer distance is getting larger by ~0.4 Å. These trends agree well with the large atomic radius of Pb atoms. Indeed, the calculated metal-sulfur bond lengths in the bulk of PbS and MoS$_2$ are: 2.94 Å for Pb-S and 2.40 Å for Mo-S, while the length of the covalent Pb-S bond within Pb-doped MoS$_2$ lattice is 2.65 Å.

Furthermore, the influence of the concentration and ordering of the impurity atoms on the thermodynamic stability of doped Mo$_{1-x}$Pb$_x$S$_2$ and intercalated Pb$_y$/MoS$_2$ phases can be considered. To characterize the stability of Mo$_{1-x}$Pb$_x$S$_2$ and the Pb$_y$/MoS$_2$ phases, the cohesion energies E_{coh} were calculated for a set of 4 × 4 × 1 2H-MoS$_2$ supercells modified by 1–4 Mo atoms (Table 1). In agreement with the picture of the electronic structure, the absolute values of E_{coh} for all modified systems vanish with the growing content of Pb, which is an evidence for the weakening of chemical bonding in both doped and intercalated MoS$_2$ compared to the pristine MoS$_2$. Noteworthy, the cohesion energies of the solid solutions as well as intercalates vary almost in the same order of magnitude, and the competing formation of both phases during the Pb-promoted growth of MoS$_2$ nanotubes can be anticipated.

The exact growth mechanism and the main compounds participating in the growth of MoS$_2$ nanotubes have still to be found. Yet, a first insight in this process is possible by the consideration of some model reactions. The formation energies ΔE for Mo$_{1-x}$Pb$_x$S$_2$ and Pb$_y$/MoS$_2$ phases from MoS$_2$ and the corresponding compounds were estimated using calculated change in the total energies of the next formal reactions:

$$(1 - x)\,\text{MoS}_2 + x\text{PbS} + x\text{S} = \text{Mo}_{1-x}\text{Pb}_x\text{S}_2 \tag{1}$$

$$y\text{Pb} + \text{MoS}_2 = \text{Pb}_y/\text{MoS}_2 \tag{2}$$

Both reactions have been found to be highly endothermic (Table 2). Concerning the calculated values of ΔE, a strong tendency for the phase separation of Pb-modified MoS$_2$ lattice into a mixture of simple binary sulfides and simple elements may be contemplated. These theoretical observations are in agreement with the experimental finding of the time-depended Pb content in fabricated MoS$_2$ samples.

Table 2. Cohesion energies E_{coh} and energies of formation ΔE of $Mo_{1-x}Pb_xS_2$ solid solutions and Pb_y/MoS_2 intercalates concerning reactions (1) and (2), as a function of the content and the arrangement of Pb atoms within model supercells. LDA DFT calculations.

Isomer	Pb atoms Arrangement	Supercell Composition	E_{coh}, eV/atom	ΔE, eV/Pb
	no Pb atoms	$Mo_{32}S_{64}$, $x,y = 0.00$	−1.58	-
	$Mo_{1-x}Pb_xS_2$ Doped by			
D1	single Pb atom	$Pb_1Mo_{31}S_{64}$, $x = 0.031$	−1.50	4.65
D2a	two neighbor Pb atoms within the same layer	$Pb_2Mo_{30}S_{64}$, $x = 0.063$	−1.45	3.75
D2b	two distant Pb atoms within the same layer	$Pb_2Mo_{30}S_{64}$, $x = 0.063$	−1.43	4.63
D2c	two neighbor Pb atoms in different layers	$Pb_2Mo_{30}S_{64}$, $x = 0.063$	−1.43	4.42
D2d	two distant Pb atoms in different layers	$Pb_2Mo_{30}S_{64}$, $x = 0.063$	−1.43	4.46
D3a	three neighbor Pb atoms within the same layer	$Pb_3Mo_{29}S_{64}$, $x = 0.094$	−1.39	3.34
D4a	four neighbor Pb atoms within the same layer	$Pb_4Mo_{28}S_{64}$, $x = 0.125$	−1.33	3.18
	Pb_y/MoS_2 Intercalated by			
I1	single Pb atom	$Pb_1/Mo_{32}S_{64}$, $y = 0.031$	−1.51	5.72
I2a	two neighbor Pb atoms within the same vdW gap	$Pb_2/Mo_{32}S_{64}$, $y = 0.063$	−1.47	3.79
I2b	two distant Pb atoms within the same vdW gap	$Pb_2/Mo_{32}S_{64}$, $y = 0.063$	−1.46	4.28
I2c	two neighbor Pb atoms in different vdW gaps	$Pb_2/Mo_{32}S_{64}$, $y = 0.063$	−1.44	5.66
I2d	two distant Pb atoms in different vdW gaps	$Pb_2/Mo_{32}S_{64}$, $y = 0.063$	−1.43	5.73

Noteworthy, the formation energies for the model supercells with "associated" (neighboring) Pb atoms in both Pb-doped and Pb-intercalated MoS_2 are considerably lower, than for those supercells, where all Pb atoms are separated. e.g., the interaction between two Pb atoms separated by the distance ~6.3 Å in $Mo_{1-x}Pb_xS_2$ solid solutions is almost absent (ΔE for D2b and D2c isomers are close to that of D1, Table 1). The same tendency can be obtained in Pb_y/MoS_2 intercalates, yet, with a higher range of interaction between Pb atoms (ΔE for I2b isomer is still less, than for I1, Table 1). Thus, the solid solutions of $Mo_{1-x}Pb_xS_2$ should be more stable than Pb_y/MoS_2 intercalates, since the coalescence of intercalated Pb atoms is more favorable and Pb_y/MoS_2 intercalates might exist in the narrower part of the phase diagram at a lower Pb content, than $Mo_{1-x}Pb_xS_2$ solid solutions.

Concerning the analysis of calculated formation energies for the case of single doping or intercalating Pb atoms, the formation of $Mo_{1-x}Pb_xS_2$ solid solutions is more likely, than the formation of Pb_y/MoS_2 intercalates. As well, the values of formation energies allow an estimation of the limit of the lead solubility at certain temperature T at thermodynamic equilibrium. As example, we consider roughly the possible content within $Mo_{1-x}Pb_xS_2$ compounds after reaction (1). The preference of one of two

states in a chemical reaction is determined by the free energy change $\Delta F = \Delta U - T\Delta S$, where ΔU is the change of internal energy, ΔS is the change of entropy. The condition corresponding to the phase separation is $\Delta F \leq 0$.

In the first approximation, ΔS can be defined as the configurational entropy of randomly distributed Pb atoms in the metal sublattice of $Mo_{1-x}Pb_xS_2$. From the theory of ideal solutions it follows, that

$$\Delta S = R\left(\ln x + \frac{(1-x)}{x}\ln(1-x) \right) \tag{3}$$

where ΔS is expressed per mole of Pb. ΔU can be approximated as the energy of reaction (1) ($\Delta U = \Delta E$). The estimation of the free energy change for the phase separation within $Mo_{1-x}Pb_xS_2$ solid solutions with a fortiori low x imply the use of the energy for the formation of single Pb atom within MoS_2 lattice, *i.e.*, $\Delta E = 4.65$ eV or 448.7 kJ/Pb-mol (isomer D1, Table 1).

The results of this approach based on the formal reaction (1) are visualized in Figure 6. They reveal that the substitution of Pb atom instead of the Mo atom within the MoS_2 lattice is a quite rare event and the content of Pb at thermodynamic equilibrium would be around $x = 10^{-7}$ at the temperatures ~3000 K. In this manner, the experimentally fabricated MoS_2 nanotube samples with primary Pb content of $x = 0.12$, which were formed during the extreme reaction conditions of the sun-light driven evaporation, are thermodynamically unstable and should show a high urge towards a phase separation.

Figure 6. Calculated free energy ΔF of the phase separation within $Mo_{1-x}Pb_xS_2$ solid solutions depending on the temperature and Pb content (x).
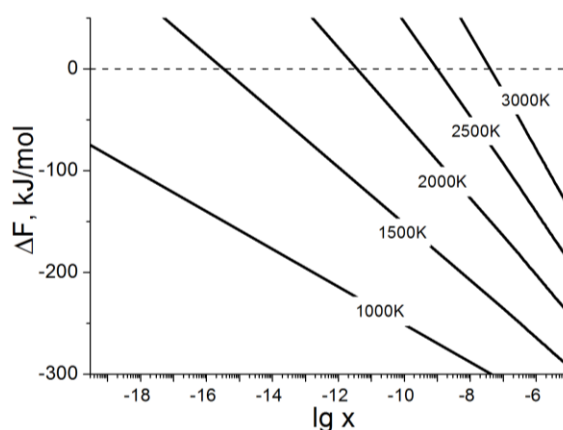
3. Experimental Section

MoO_{3-x} nanowhiskers and MoS_2 nanotubes were prepared using solar ablation system [15]. The Pb and MoS_2 mixture was sealed in a quartz ampoule and irradiated using solar ablation system for 30 s in the case of MoO_{3-x} nanowhiskers, and for 10 min in the case of MoS_2 nanotubes. Both nanostructures contain a few atomic percent of Pb. After spending a year in ambient conditions these samples were annealed at 810 °C in the presence of H_2S and forming gas (5% H_2 and 95% N_2). The annealing time varied from 30 min to 2 h. The sample labeling can be seen in Table 2.

At each stage the samples were examined with a transmission electron microscope (TEM) operating at 120 kV, equipped with an energy-dispersive X-ray spectroscopy (EDS) detector for chemical

analysis. The SEM image was generated using a scanning electron microscope (SEM), and high-resolution imaging was achieved with a field-emission gun TEM operating at 300 kV.

The calculations were performed using the SIESTA 2.0 (Madrid, Spain) implementation [23,24] within the framework of density-functional theory (DFT) [25]. The exchange-correlation potential within the local-density approximation (LDA) with the Perdew-Zunger parametrization was used [26]. The core electrons were treated within the frozen core approximation, applying norm-conserving Troullier-Martins pseudopotentials [27]. The valence electrons were taken as $3s^2 3p^4$ for S, $4d^5 5s^1 5p^0$ for Mo, $6s^2 6p^2$ for Pb, while $Pb5d^{10}$ electrons were included as semi-core state. The pseudopotential core radii were chosen, as suggested by Martins, and are equal to 1.70 a_B for all S states, 2.45 a_B for Mo$4d$ and Mo$5s$, 2.65 a_B for Mo$5p$ states, 3.20 a_B for Pb$6s$ and Pb$6p$, 3.00 a_B for Pb$5d$ states. In all calculations double-ζ basis set is used for all atoms. For *k*-point sampling, a cutoff of 10 Å was used [28]. The *k*-point mesh was generated by the method of Monkhorst and Pack [29]. The real-space grid used for the numeric integrations was set to correspond to the energy cutoff of 300 Ry. For the study of substitutional doping and intercalation of MoS_2 by Pb atoms the supercell of $4 \times 4 \times 1$ of 2H-MoS_2 unit cells was considered. The energies of chemical reactions were estimated from the calculations of total energies for 2H-MoS_2, bcc-Mo, fcc-Pb, fcc-PbS and molecular S_8. All calculations were performed using variable-cell and atomic position relaxation, with convergence criteria set to correspond to a maximum residual stress of 0.1 GPa for each component of the stress tensor, and maximum residual force component of 0.01 eV/Å.

4. Conclusions

The experimental work shows that MoO_{3-x} (1) nanowhiskers and MoS_2 (1) nanotubes synthesized using solar ablation system, are stable for more than a year in the ambient conditions. However, Pb atoms that were observed in these nanostructures, are not stable in high concentration and tend to diffuse out of the lattice. The Pb outdiffusion from these nanostructures did not influence their high-temperature stability and their conversion into MoS_2 (3,4) nanotubes. In all cases MoS_2 nanotubes were observed after the sulfidization and annealing of MoO_{3-x} (2) nanowhiskers and MoS_2 (2) nanotubes. According to the EDS measurements the initial Pb concentration in both nanostructures was reduced after one year in the drawer. While subsequent annealing of these nanostructures lead to additional reduction of their Pb concentration. It can be seen from the EDS spectra that in the case of molybdenum suboxide nanowhiskers MoO_{3-x} (2) as a precursor material, the Pb peak disappears after two hours (H_2S) annealing, while the same peak disappears after 30 min annealing at 810 °C in the case of MoS_2 (2) nanotubes.

DFT calculations have verified a very low affinity of Pb atoms as either substitutional or intercalating agents to the host MoS_2 lattice. Both types of modifications should lead to the destabilization of the electronic structure of the pristine MoS_2 and cause a weak chemical bonding between Pb and S atoms with the oxidation state of Pb^{2+}. The calculations have also demonstrated that the interaction between Pb atoms as intercalates is slightly stronger, than the interaction between Pb atoms as substitutional dopants in the MoS_2 lattice. Thus, Pb_y/MoS_2 intercalates might exist only at lower Pb content compared to a solid solution of $Mo_{1-x}Pb_xS_2$. The latter phase seems to be a more favorite form of Pb within the fabricated MoS_2 nanotubes. The estimations of the free energies for the phase

separation of $Mo_{1-x}Pb_xS_2$ solid solutions explain the experimentally observed time- and high-temperature reduction of the Pb content in the nanotube lattice. The experimentally reached Pb concentrations ($x = 0.3$) may be attributed to a thermodynamically unstable system which was obtained by a fast kinetic of the chemical reaction between lead atoms and the primary $2H$-MoS_2 lattice during the solar ablation experiments.

Acknowledgments

Author Contributions

Olga Brontvein and Reshef Tenne designed the research. Olga Brontvein recorded and analyzed TEM, SEM and EDS data. Andrey Enyashin carried out DFT calculations. The manuscript was written through contributions of all authors. All authors have given approval to the final version of the manuscript.

Conflicts of Interest

The authors declare no conflict of interest.

References

1. Kaplan-Ashiri, I.; Cohen, S.; Gartsman, K.; Rosentsveig, R.; Seifert, G.; Tenne, R. Mechanical behavior of individual WS_2 nanotubes. *J. Mater. Res*. **2004**, *19*, 454–459.
2. Kaplan-Ashiri, I.; Cohen, S.R.; Gartsman, K.; Ivanovskaya, V.; Heine, T.; Seifert, G.; Wiesel, I.; Wagner, H.; Tenne, R. On the mechanical behavior of WS_2 nanotubes under axial tension and compression. *Proc. Natl. Acad. Sci. USA* **2006**, *103*, 523.
3. Nagapriya, K.S.; Goldbart, O.; Kaplan-Ashiri, I.; Seifert, G.; Tenne, R.; Joselevich, E. Torsional stick-slip behavior in WS_2 nanotubes. *Phys. Rev. Lett.* **2008**, *101*, 195501.
4. Frey, G.L.; Tenne, R.; Matthews, M.J.; Dresselhaus, M.S.; Dresselhaus, G. Optical properties of MS_2 (M = Mo, W) inorganic fullerenelike and nanotube material optical absorption and resonance raman measurements. *J. Mater. Res*. **1998**, *13*, 2412–2417.
5. Staiger, M.; Rafailov, P.; Gartsman, K.; Telg, H.; Krause, M.; Radovsky, G.; Zak, A.; Thomsen, C. Excitonic resonances in WS_2 nanotubes. *Phys. Rev. B* **2012**, *86*, doi:10.1103/PhysRevB.86.165423.
6. Virsek, M.; Jesih, A.; Milosevic, I.; Damnjanovic, M.; Remskar, M. Raman scattering of the MoS_2 and WS_2 single nanotubes. *Surf. Sci*. **2007**, *601*, 2868–2872.

7. Enyashin, A.; Gemming, S.; Seifert, G. Nanosized allotropes of molybdenum disulfide. *Eur. Phys. J.-Spec. Top.* **2007**, *149*, 103–125.

8. Levi, R.; Bitton, O.; Leitus, G.; Tenne, R.; Joselevich, E. Field-effect transistors based on WS_2 nanotubes with high current-carrying capacity. *Nano Lett*. **2013**, *13*, 3736–3741.

9. Remskar, M.; Skraba, Z.; Cleton, F.; Sanjines, R.; Levy, F. MoS_2 as microtubes. *Appl. Phys. Lett.* **1996**, *69*, 351–353.

10. Remskar, M.; Mrzel, A.; Virsek, M.; Godec, M.; Krause, M.; Kolitsch, A.; Singh, A.; Seabaugh, A. The MoS_2 nanotubes with defect-controlled electric properties. *Nanoscale Res. Lett.* **2010**, *6*, 26.

11. Yella, A.; Mugnaioli, E.; Panthöfer, M.; Therese, H.A.; Kolb, U.; Tremel, W. Bismuth-catalyzed growth of SnS_2 nanotubes and their stability. *Angew. Chem. Int. Ed.* **2009**, *48*, 6426–6430.

12. Radovsky, G.; Popovitz-Biro, R.; Stroppa, D.G.; Houben, L.; Tenne, R. Nanotubes from chalcogenide misfit compounds: Sn–S and Nb–Pb–S. *Acc. Chem. Res*. **2013**, *47*, 406–416.

13. Radovsky, G.; Popovitz-Biro, R.; Staiger, M.; Gartsman, K.; Thomsen, C.; Lorenz, T.; Seifert, G.; Tenne, R. Synthesis of copious amounts of SnS_2 and SnS_2/SnS nanotubes with ordered superstructures. *Angew. Chem. Int. Ed*. **2011**, *50*, 12316–12320.

14. Zak, A.; Sallacan-Ecker, L.; Margolin, A.; Genut, M.; Tenne, R. Insight into the growth mechanism of WS_2 nanotubes in the scaled-up fluidized bed reactor. *Nano* **2009**, *4*, 91–98.

15. Brontvein, O.; Stroppa, D.G.; Popovitz-Biro, R.; Albu-Yaron, A.; Levy, M.; Feuerman, D.; Houben, L.; Tenne, R.; Gordon, J.M. New high-temperature Pb-catalyzed synthesis of inorganic nanotubes. *J. Am. Chem. Soc*. **2012**, *134*, 16379–16386.

16. Brontvein, O.; Jayaram, V.; Reddy, K.P.J.; Gordon, J.M.; Tenne, R. Two-step synthesis of MoS_2 nanotubes using shock waves with lead as growth promoter. *Z. Anorg. Allg. Chem.* **2014**, *640*, 1152–1158.

17. Feldman, Y.; Wasserman, E.; Srolovitz, D.; Tenne, R. High-rate, gas-phase growth of MoS_2 nested inorganic fullerenes and nanotubes. *Science* **1995**, *267*, 222–225.

18. Yamazoe, N.; Kihlborg, L. Mo_5O_{14}—Twinning and three-dimensional structure, determined from a partly tantalum-substituted crystal. *Acta Crystallogr. Sect. B* **1975**, *31*, 1666–1672.

19. Yamazoe, N.; Ekstrom, T.; Kihlborg, L. Structural effects of vanadium substitution in molybdenum oxide ($Mo_{17}O_{47}$). *Acta Chem. Scand. Ser. A* **1975**, *29*, 404–408.

20. Kihlborg, L. Stabilization of the tunnel structure of molybdenum oxide (Mo_5O_{14}) by partial metal atom substitution. *Acta Chem. Scand.* **1969**, *23*, 1834–1835.

21. Boker, T.; Severin, R.; Muller, A.; Janowitz, C.; Manzke, R.; Voss, D.; Kruger, P.; Mazur, A.; Pollmann, J. Band structure of MoS_2, $MoSe_2$, and α-$MoTe_2$: Angle-resolved photoelectron spectroscopy and *ab initio* calculations. *Phys. Rev. B* **2001**, *64*, 235305.

22. Walsh, A. Effects of reduced dimensionality on the electronic structure and defect chemistry of semiconducting hybrid organic-inorganic PbS solids. *Proc. R. Soc. A* **2011**, *467*, 1970–1985.

23. Ordejon, P.; Artacho, E.; Soler, J.M. Self-consistent order-N density-functional calculations for very large systems. *Phys. Rev. B* **1996**, *53*, 10441–10444.

24. Soler, J.M.; Artacho, E.; Gale, J.D.; Garcia, A.; Junquera, J.; Ordejon, P.; Sanchez-Portal, D. The SIESTA method for *ab initio* order-N materials simulation. *J. Phys.-Condens. Matter* **2002**, *14*, 2745–2779.

25. Hohenberg, P.; Kohn, W. Inhomogeneous electron gas. *Phys. Rev.* **1964**, *136*, B864–B871.

26. Perdew, J.P.; Zunger, A. Self-interaction correction to density-functional approximations for many-electron systems. *Phys. Rev. B* **1981**, *23*, 5048–5079.

27. Troullier, N.; Martins, J.L. Efficient pseudopotentials for plane-wave calculations. *Phys. Rev. B* **1991**, *43*, 1993–2006.

28. Moreno, J.; Soler, J.M. Optimal meshes for integrals in real-space and reciprocal-space unit cells. *Phys. Rev. B* **1992**, *45*, 13891–13898.

29. Monkhorst, H.J.; Pack, J.D. Special points for Brillouin-zone integrations. *Phys. Rev. B* **1976**, *13*, 5188–5192.